Radiation Protection Dosimetry
Vol. 11 No. 3 pp. 151–157 (1985)
Nuclear Technology Publishing

THE EFFECT OF ALTITUDE ON BETA RAY SOURCE CALIBRATIONS

J. S. Pruitt
Center for Radiation Research
National Bureau of Standards
Gaithersburg, MD 20899, USA

Received September 19 1984, Amended March 20 1985, Accepted March 24 1985

Abstract — A study has been made of the effect of altitude on beta ray source calibrations, using commercially available ^{147}Pm, ^{204}Tl, and $^{90}Sr+^{90}Y$ sources. The measurements were made in a large environmental chamber, from which air was removed to simulate several altitudes between sea-level and 3.7 km (12,000 feet). The results show that the calibration does vary with altitude, most drastically for ^{147}Pm, much less for both ^{204}Tl and $^{90}Sr+^{90}Y$. It is shown that the change in source calibration for a given change in air density is almost the same as the change produced by addition of a plastic filter with the same thickness in mass per unit area.

INTRODUCTION

Institutions in several countries have purchased sets of calibrated beta ray sources from a supplier who provides calibration certificates from measurements of absorbed dose rates made at sea-level. Some of the calibration results are functions of the density of the air between source and detector, which can differ by more than 20% between laboratories at high altitudes and those at sea-level. The variation with air density is a function of the beta ray spectrum and consequently depends on the radionuclide, the encapsulation, the flattening filter, and the mass per unit area of absorber in front of the detector.

The measurements described in this report were made to investigate the air density dependence for a calibrated set of four beta ray sources purchased from Buchler Gmbh & Co. of Braunschweig, FRG*. There are three different nuclides, chosen from the 1981 recommendations of the International Organisation for Standardisation[1], ^{147}Pm, ^{204}Tl, and $^{90}Sr+^{90}Y$, which cover a range of maximum energies from 0.2 MeV to 2.3 MeV. The results of this study should also be applicable to similar sets of sources calibrated and distributed about 10 years ago by the National Physical Laboratory (Teddington, Middlesex, England)[2,3].

The instruction booklet accompanying the Buchler sources recognises the need to correct absorbed dose rates for air density variations, and supplies correction factors for use with densities which differ by no more than ±2% from the density at the reference conditions (20°C and 101.3 kPa). It is not

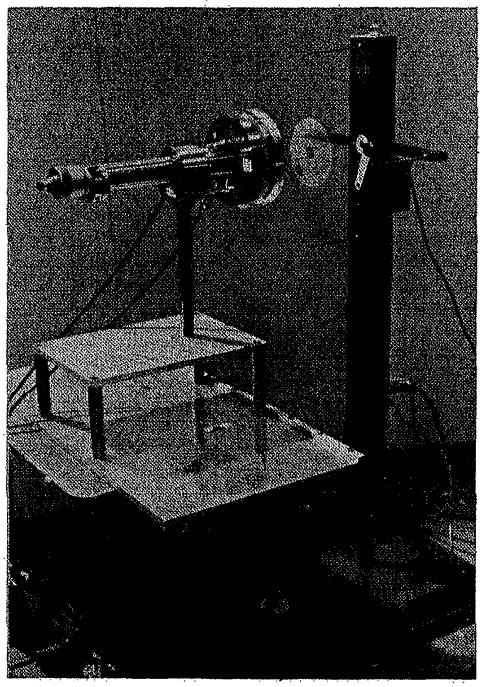

Figure 1. Experimental equipment, showing source holder and filter on the right and extrapolation ionisation chamber on the left.

*Commercial product identification does not imply a recommendation or endorsement by NBS, nor does it imply that NBS considers the identified products to be the best available for the purpose.

expected that these factors would be valid for air density changes as large as 20%.

The measurements consist of determinations of ionisation current from an extrapolation ionisation chamber placed at the calibration position, and a study of how this current varies with air density. Since the normal range of air density variation caused by weather changes at our laboratory is only a few per cent, the measurements were made in an environmental chamber where the air density was varied at will over a much larger range, simulating altitudes between sea-level and about 3.7 km (12,000 feet).

THE EXPERIMENT

Pertinent data about the four beta ray sources are listed in Table 1. Sources 3 and 4 are both strontium+yttrium and share many characteristics, but have different activities. The sources and filters are supported on the stand shown at the right in Figure 1. The filter shown is for ^{147}Pm, mounted 10 cm downstream from the source. The shutter is shown in the open position in Figure 1.

The instrument at the left in Figure 1, mounted on the cart, is the extrapolation chamber. This was constructed at the Physikalisch-Technische Werkstätten (Freiburg, FRG) using plans from the Physikalisch-Technische Bundesanstalt (Braunschweig, FRG)[4,5]. Figure 2 shows a cross section of the front end of this chamber. The piston is polymethylmethacrylate (PMMA) with a graphite coating with an inscribed 30 mm diameter collecting electrode and a 15 mm wide guard ring. The polarising electrode is 2.6 mg.cm^{-2} of graphite-coated polyethylene terepthalate foil. The electrode separation can be both measured and controlled with a micrometer screw graduated in hundredths of a millimeter. It was set at 2.5 mm for these experiments, and the polarising voltage used was ±25 V.

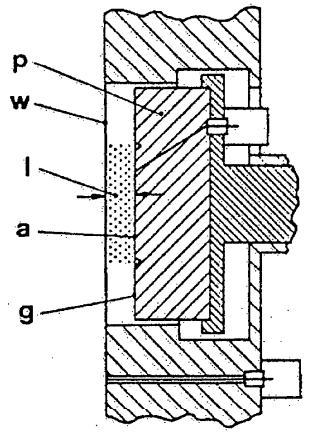

Figure 2. Cross section of the main parts of the extrapolation chamber, showing the piston (p), the entrance window (w), the air gap (l), the collecting electrode area (a), and the guard ring (g). The effective measuring volume is stippled.

The ion current was measured with a sensitive electrometer-digital voltmeter system using the capacitative rate-of-charge method. For each data set reported below, the current is the average of three measurements with positive polarity and three with negative polarity. The reported currents have been corrected for (1) departure from a reference air temperature and pressure of 22°C and 101.3 kPa (using the factor 101.325 (T+275.15)/(295.15P), where T is temperature in degrees Celsius and P is pressure in kilopascals), (2) source decay, (3) scatter from the side walls of the extrapolation chamber[6], (4) ion recombination and diffusion[7], and (5) in the case of ^{147}Pm, a factor (taken from the manual supplied with the source) of 1.02 exp ($-4.37 \times 10^{-4} \times$ % relative humidity).

The initial measurements with each source were

Table 1. Characteristics of the Buchler beta ray sources.

	Source number			
	1	2	3	4
Radionuclide	^{147}Pm	^{204}Tl	^{90}Sr+^{90}Y	
Max. energy (MeV)	0.23	0.76	2.3	
Mean energy (MeV)	0.06	0.24	0.8	
Half life (years)	2.62	3.78	28.5	
Nominal activity (MBq)	500	20	80	2000
Encapsulation	5 mg.cm^{-2} Ag +0.5 mg.cm^{-2} Ni	20 mg.cm^{-2} Ag +1 mg.cm^{-2} Au	50 mg.cm^{-2} Ag +80 mg.cm^{-2} Fe	50 mg.cm^{-2} Ag +80 mg.cm^{-2} Fe
Flattening filter	yes	yes	yes	no
Calibration distance (mm)	200	300	300	300
Tissue dose rate* (μGy.s^{-1})	0.28	0.35	1.88	69

*Surface dose rates at the time of calibration in Sept-Oct. 1982.

made with no absorbers in front of the extrapolation chamber (front wall thickness 2.6 mg.cm^{-2}), but in later measurements polyethylene terepthalate absorbers up to 43.6 mg.cm^{-2} were added. In one case, with source 4, a 315.2 mg.cm^{-2} polystyrene absorber was added to the chamber. The absorber thicknesses used were chosen arbitrarily to study the air density dependence in several regions of each depth-dose curve.

THE ENVIRONMENTAL CHAMBER

The current measurements were made inside a walk-in environmental chamber at the Aerosol Studies Division of the US Department of Energy Environmental Measurements Laboratory in New York City. This chamber had inside floor dimensions of 1.8 m × 3.0 m and a height of 2.0 m. With the source-extrapolation chamber unit centred, the scattering surface closest to both the extrapolation chamber and the source was the floor, just as it would be in a low-scatter room. The distance of the floor from the source-chamber axis was 0.76 m.

A pump was used both for removing air from the environmental chamber and for air leakage compensation. The latter operation was performed by an automatic cycling mechanism that maintained the pressure within ±0.4 kPa. The environmental chamber also had air temperature controls, but these were used only when needed to maintain a constant temperature with change in pressure. The air density was changed either by pumping out the chamber or by letting in air through a valve.

Air pressure inside the chamber was monitored with an externally mounted aneroid barometer with a reading uncertainty of about ±0.15 kPa; internal air temperature and relative humidity were both monitored with a commercial probe connected to a digital display outside the chamber. Temperature, pressure, and relative humidity were recorded for each set of current measurements.

RESULTS

The average current determinations are plotted in Figures 3 to 6 for the four sources. Each point represents the corrected average of the results of from 2 to 9 sets of data as defined in the Introduction. The results are plotted as a function of the relative air density, ρ/ρ_0, where ρ is the air density during the experiment and ρ_0 is its value at the reference temperature and pressure of 22°C and 101.3 kPa (note that the reference temperature differs from that cited for the source manual). It can be seen that the change of current with air density is most pronounced for the source with the lowest average beta ray energy, ^{147}Pm, and decreases in magnitude for higher energy beta rays.

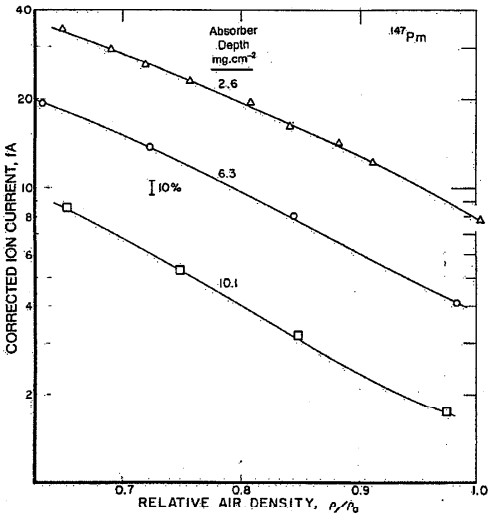

Figure 3. Corrected extrapolation chamber current as a function of relative air density for the ^{147}Pm source, with and without polyethylene terepthalate absorbers added to the chamber face.

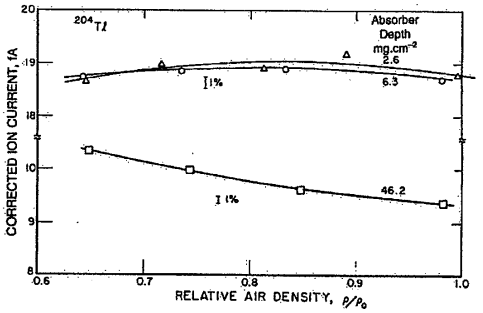

Figure 4. Corrected extrapolation chamber current as a function of relative air density for the ^{204}Tl source, with and without polyethylene terepthalate absorbers added to the chamber face.

The precision of the measurements was not as high as can be obtained with the extrapolation chamber-electrometer system when used under ideal conditions. The principal source of error was vibration from the pump used to control air pressure in the environmental chamber, since the low-noise extrapolation chamber signal cable was still somewhat microphonic. The earliest measurements were made at 2.6 mg.cm^{-2} with the ^{147}Pm, ^{204}Tl, and 80 MBq ^{90}Sr+^{90}Y sources, before the best mechanical isolation had been attained. It can be seen that the random fluctuations were larger in these three cases.

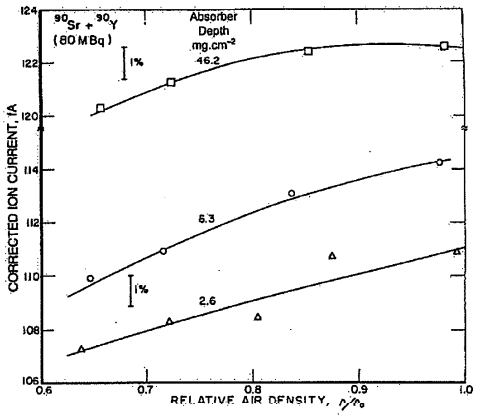

Figure 5. Corrected extrapolation chamber current as a function of relative air density for the 80 MBq $^{90}Sr+^{90}Y$ source, with and without polyethylene terepthalate absorbers added to the chamber face.

The curves drawn in Figures 3 to 6 are all least-squares parabolas. The coefficients of these parabolas, expressed as functions of the dimensionless variable $x = 1 - \rho/\rho_0$ the (quantity x is small near the reference conditions and increases with increasing altitude) and normalised at the reference conditions, are given in Table 2, along with the root-mean-square deviations σ. These coefficients may be of some use in practical applications, but it should be remembered that this description is purely empirical.

The curves of Figures 3 to 6 differ greatly in slope, which can be explained qualitatively by considering that a decrease in air density is equivalent to a decrease in source distance if the $1/r^2$ change is ignored. For $^{90}Sr+^{90}Y$, there is a build-up near the source caused by scattered beta rays. This build-up has not yet reached its peak at the 300 mm source distance so that a decrease in air density also decreases the current. For ^{147}Pm, the current is dropping rapidly with distance at 200 mm because of attenuation, and an air density decrease increases the current. For ^{204}Tl, neither scatter nor attenuation is appreciable at 300 mm, and the current is almost independent of air density.

The current changes seen in these curves can be compared with the changes predicted by the instruction booklet, extrapolating these latter beyond their given range of a 2% density change. For a 20% air density change, the instruction booklet formulas would differ from the 2.6 mg.cm^{-2} curves in Figures 3 to 6 by 2% for $^{90}Sr+^{90}Y$, by 1% for ^{204}Tl, and by 13% for ^{147}Pm.

An alternative method of viewing the data, which demonstrates the reasons for this dependence of ion current on air density, is possible with the help of the depth-current curves of Figure 7. These were obtained from measurements at sea-level with the same sources. The sea-level curves have been replotted as solid lines in Figures 8 to 11 as functions of a new variable labelled 'combined absorber depth'. This is the sum of the mass per unit area of air between source and chamber and the mass per unit area of absorber (polyethylene terepthalate or polystyrene in this case) at the chamber face, the latter multiplied by the relative attenuation for that absorbing material. The relative attenuation is a scaling factor evaluated relative to air by W. G. Cross[8]. It is 1.02 for polyethylene terepthalate and

Table 2. Curve fit parameters for $I/I_0 = 1 + \alpha x + \beta x^2$, where $x = 1 - \rho/\rho_0$, and I_0 is the ion current at the reference conditions.

Nuclide	Nominal activity (MBq)	Absorber depth* (mg.cm^{-2})	No. of data sets	α	β	σ (%)
^{147}Pm	500	2.6	20	4.47	12.71	2
		6.3	9	3.54	19.79	3
		10.1	9	0.69	31.24	6
^{204}Tl	20	2.6	30	0.165	−0.500	0.9
		6.3	9	0.131	−0.333	0.3
		46.2	11	0.143	0.477	1.9
$^{90}Sr+^{90}Y$	80	2.6	14	−0.085	−0.027	0.6
		6.3	11	−0.054	−0.176	0.2
		46.2	10	0.040	−0.279	0.4
$^{90}Sr+^{90}Y$	2000	2.6	11	0.115	−0.502	0.3
		46.2	10	0.067	−0.181	0.2
		318**	21	0.250	−0.394	0.2

*Thickness of polyethylene terepthalate absorber in front of the extrapolation chamber air gap.
**315.2 mg.cm^{-2} of polystyrene in front of the 2.6 mg.cm^{-2} extrapolation chamber window.

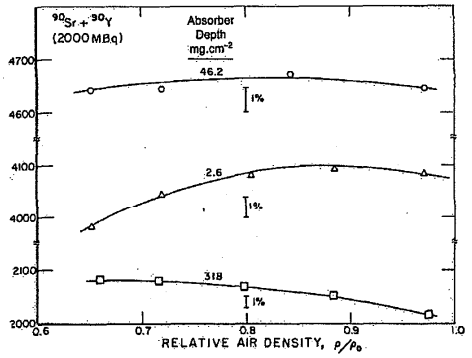

Figure 6. Corrected extrapolation chamber current as a function of relative air density for the 2000 MBq $^{90}Sr+^{90}Y$ source, with and without absorbers added to the chamber face. The 46.2 mg.cm^{-2} curve is for added polyethylene terepthalate absorbers and the 318 mg.cm^{-2} curve is for added polystyrene absorbers.

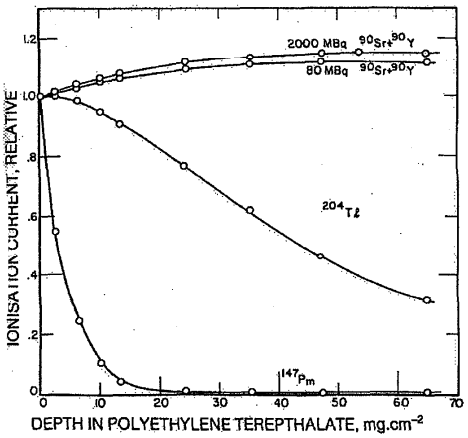

Figure 7. Normalised depth-current curves in polyethylene terepthalate for all four sources, measured at sea-level.

1.04 for polystyrene. In symbols, the combined absorber depth (CAD) is given by

$$CAD = \rho_a S + \eta_x \rho_x X \qquad (1)$$

where S is the source distance, X is the absorber thickness, ρ_a and ρ_x are densities of the air and the absorber, respectively, and η_x is the relative attenuation of the absorber. When the average current measurements of Figures 3 to 6 are also replotted as functions of combined absorber depth, it can be seen in Figures 8 to 11 that they follow the sea-level curves to within a few per cent.

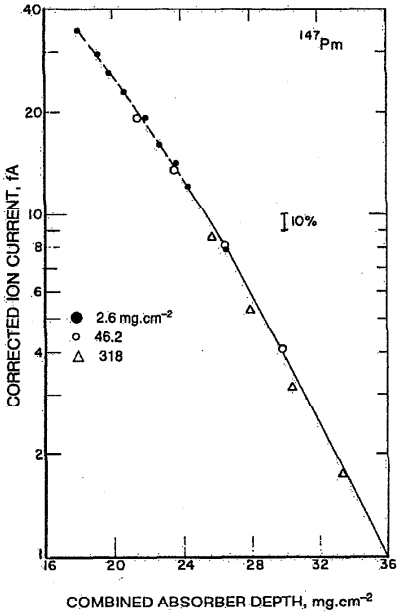

Figure 8. Comparison of sea-level depth-current curve in polyethylene terepthalate for ^{147}Pm (solid line), with data points obtained by varying air density, as a function of 'combined absorber depth'.

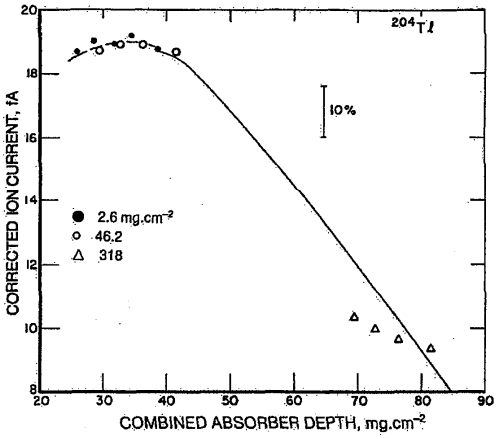

Figure 9. Comparison of sea-level depth-current curve in polyethylene terepthalate for ^{204}Tl (solid line), with data points obtained by varying air density, as a function of 'combined absorber depth'.

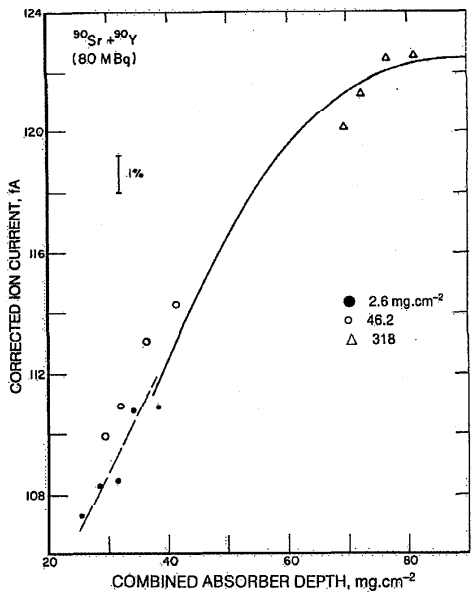

Figure 10. Comparison of sea-level depth-current curve in polyethylene terepthalate for the 80 MBq $^{90}Sr+^{90}Y$ source (solid line), with data points obtained by varying air density, as a function of 'combined absorber depth'.

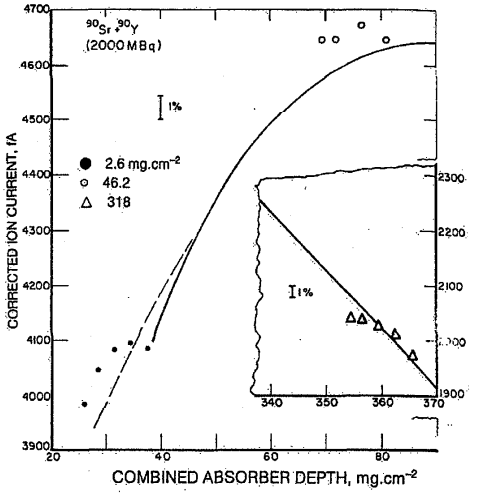

Figure 11. Comparison of sea-level depth-current curves for the 2000 MBq $^{90}Sr+^{90}Y$ source (solid lines), with data points obtained by varying air density, as a function of 'combined absorber depth'. The main curve is for polyethylene terepthalate absorbers and the inset curve is for polystyrene absorbers.

COMMENTS

The picture that emerges is that the distribution of absorbed dose in a phantom is just a continuation of the distribution in air between source and phantom, with no abrupt changes at the interface. Both parts of this distribution can be described by a single curve, which remains approximately the same when either the air density or the absorber thickness is changed (although the source distance must remain fixed to avoid solid angle changes). This suggests a simple method for determining the air density dependence for an arbitrary source calibrated at sea-level if the source is supplied with depth-dose data in tissue. Each tissue depth must first be converted to combined absorber depth using Equation 1, with ρ_a equal to the air density at the pressure and temperature specified in the calibration certificate, and η_x, ρ_x, and X all referring to tissue. According to Cross, $\rho_x = 1.11$ for tissue ('muscle')[8]. When the depth-dose data are plotted as a function of combined absorber depth, the curve can be used with Equation 1 to predict the relative dose rate for arbitrary air densities and absorber thicknesses. For thin absorbers and/or high altitudes, it may be necessary to extrapolate the curve toward low CAD, as has been done in Figures 8 to 11.

The Buchler sources described in this report were supplied with depth-dose data in tissue and, using the above technique, it was found that these data agree with the solid curves of Figures 8 to 11 to within 1%.

The accuracy of these predictions of variation with air density may best be judged from Figures 8 to 11. These indicate the presence of systematic differences between the effects of varying ρ_a (individual points) and varying X (solid curves). The differences seem to increase as (i) the beta ray energies decrease, or as (ii) the air density decreases. The best that can be expected is an accuracy of about 1%.

ACKNOWLEDGEMENTS

I would like to extend heartfelt thanks to the personnel of the Aerosol Studies Division of the Environmental Measurements Laboratory, who made this study possible. Particular thanks are due to Earl Knutson, who graciously granted time and space for the work, and Henry Franklin, who operated the pumping system and provided both moral and logistical support. Thanks are also due to Margarete Ehrlich of this laboratory for suggesting the study and arranging for the use of the environmental chamber, and to Robert Loevinger for suggesting the use of 'combined absorber depth'.

REFERENCES

1. International Organization for Standardization. *Reference Beta Radiations for Calibrating Dosemeters and Doseratemeters and for Determining Their Response as a Function of Beta Radiation Energy,* ISO/DIS 6980 (1983). Available from the American National Standards Institute, New York, NY.
2. Rossiter, M. J. *The Calibration Hierarchy for Beta Dosimetry.* IN Third Information Seminar on the Radiation Protection Dosimeter Intercomparison Programme. Report of the Commission of the European Communities EUR 7365 EN, p. 128 (Brussels: Office for Official Publication of the European Communities)
3. Owen, B. *The Beta Calibration of Radiation Survey Instruments at Protection Levels.* Phys. Med. Biol. **17**, 175 (1972).
4. Böhm, J. Report KFK 2185 (Kernforschungszentrum Karlsruhe) p. 31 (1975).
5. Böhm J. *Standardization and Calibration in Beta Dosimetry.* IN Proceedings of the International Beta Dosimetry Symposium, Washington, 15-18 Feb. 1983. NUREG/CP-0050, p. 73 (US Nuclear Regulatory Commission, Washington, DC 20555) (1984).
6. Böhm, J. *The Perturbation Correction Factor of Ionization Chambers in β-Radiation Fields.* Phys. Med. Biol. **25**, 65 (1980).
7. Böhm, J. *Saturation Corrections for Plane-Parallel Ionization Chambers.* Phys. Med. Biol. **21**, 754 (1976).
8. Cross, W. G. *Variation of Beta Dose Attenuation in Different Media.* Phys. Med. Biol. **13**, 611 (1968).